Modeling of particle imaging through shock waves

Gerrit E. Elsinga, Bas W. van Oudheusden, Fulvio Scarano

Delft University of Technology, Dept. of Aerospace Eng.
PO Box 5058, 2600 GB Delft, The Netherlands
phone: +31 15 2786386 fax: +31 15 2787077
email: G.E.Elsinga@lr.tudelft.nl
B.W.vanOudheusden@lr.tudelft.nl
F.Scarano@lr.tudelft.nl

ABSTRACT

In compressible flows particle imaging, as done in Particle Image Velocimetry (PIV), is far from trivial. The inhomogeneous refractive index field can cause aero-optical aberrations including blurring of the image, especially near optical interfaces such as shock waves. The understanding of the process causing particle image blur (or blurring of the point spread function of the imaging system) is important in order to assess the measurement accuracy of optical measurement systems, such as PIV. A model for imaging through a shock wave is presented to determine the characteristic shape of blurred particle images when imaged across shock waves. The conjectured model is validated through a PIV experiment, where particle image recordings of the flow across a steady oblique shock wave are obtained in a supersonic wind tunnel. The parametric study focuses on two dominating parameters: 1) the angle between the viewing axis and the shock wave; 2) the numerical aperture of the imaging optics.

Keywords: Aero-optics, Shock waves, PIV, Point spread function, Particle image blur

1. INTRODUCTION

The performance of optical measurement techniques in compressible flows can be limited by the inhomogeneous refractive index field, which is proportional to the local density, around the wind tunnel model immersed in the flow or around a flying aircraft in case of airborne optical systems. Aero-optical aberrations, including amplitude wave variation, phase distortion (blurring of the image) and light beam deflection (Sutton 1985), become most severe with increasing compressibility effects and especially in the supersonic flow regime. Optical interfaces such as shock waves can cause a strong distortion in the image, as for instance reported by Raffel and Kost 1998, Abart et al. 2004 and Elsinga et al. 2005 after observing particle images in Particle Image Velocimetry (PIV) wind tunnel experiments (Figure 1). The flow is seeded with particles, which are small (sub micrometer scale) compared to the diffraction spot of the imaging system, therefore the particle images may be directly regarded as the point-spread-function (PSF) of the imaging system together with the effects of the flow. The PIV technique is based on the concept that flow tracers immersed in the flow are imaged at two time instants in short sequence. The measurement of the tracers motion by means of spatial cross-correlation of the digital recordings of the particle images allows to infer the local flow velocity (Raffel et al 1998). The underlying hypothesis for an accurate measurement is that the optical magnification of the system is uniform or known. Any change in magnification due to an index of refraction spatial variation inevitably introduces an uncertainty in the determination of the particles displacement and in turn of the flow velocity. The error introduced by index of refraction variations is particularly sever when the refractive index gradient is aligned with the velocity gradient as discussed by Elsinga et al. (2005). Moreover, strong variations in the index of refraction such as across shock waves may introduce strong refraction and even partial reflection in proximity of the shock, which directly degrades the shape of the particle image while it travels through the flow. Such effects not only reduce the cross-correlation accuracy but decreasing the image contrast and the cross-correlation signal-to-noise ratio, they reduce the

Optical Modeling and Performance Predictions II, edited by Mark A. Kahan,
Proceedings of SPIE Vol. 5867 (SPIE, Bellingham, WA, 2005)
0277-786X/05/$15 · doi: 10.1117/12.616687

measurement confidence level. Therefore understanding of the particle image blurring, especially near shock waves, is important to assess the behavior of PIV measurement in supersonic flows.

The present study investigates the performance of optical systems imaging through planar shock waves by determining their PSF. A large number of light rays originating from a single point and propagating along different directions are traced through the flow and the imaging system using geometrical optics, i.e. Snell's law. A convolution of this geometrically constructed image with the diffraction spot for the imaging system yields the PSF. The resulting particle images showing different characteristic features are categorized into three basic types. The same conditions are generated during wind tunnel experiments in order to confirm the existence of the above mentioned categories. Finally, the effect of the observation angle with respect to the shock wave orientation and the numerical aperture is discussed.

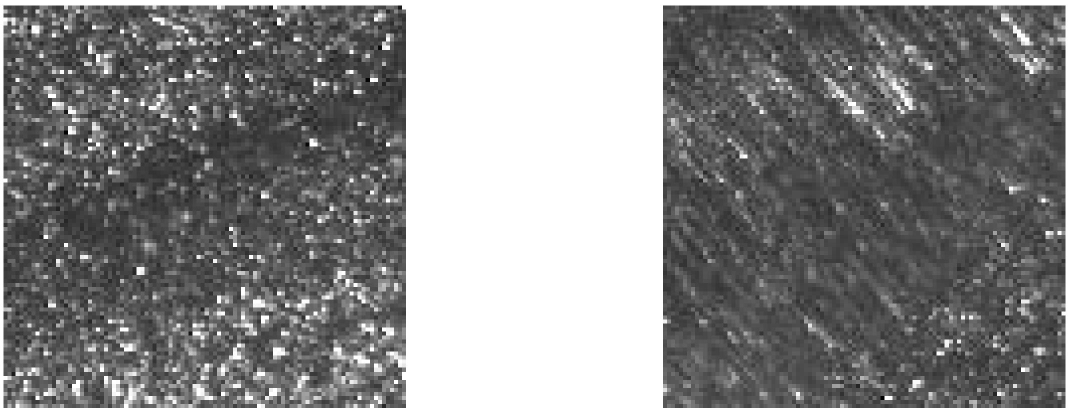

Figure 1: Particle images recorded in a uniform flow region (left) and in proximity of a shock wave (right).

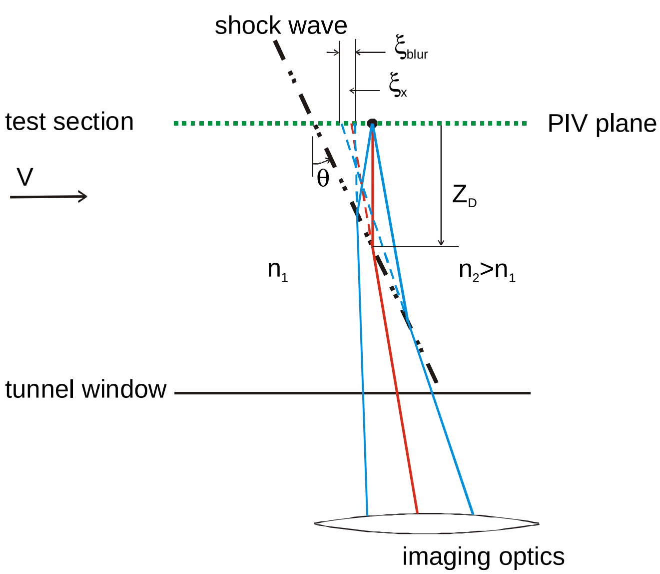

Figure 2: Model for the numerical simulation of particle imaging through shock waves. The scattered light (blue and red lines) is deflected by the shock wave.

2. IMAGING MODEL

Figure 2 schematically shows the situation to be described by the present particle imaging model. A planar shock at an angle θ with the viewing direction spans the entire wind tunnel width. Part of the scattered light by the tracer particles in the light sheet is collected by the imaging optics to form the particle image. In case a light ray intersects with the shock Snell's law applies and given the intersection angle and shock strength the deflection angle can be calculated. Because a univocal relation exists between the object in the plane of focus POF (viz. the particles within the light sheet) and the imaged particles in the image plane, the light ray position in the image is determined by a linear backward extension of the light ray (dashed lines in Figure 2) from the tunnel window (or edge of the refractive index field) to the POF, thus the magnification can be ignored. As it can be inferred from Figure 2, in presence of a shock not all light rays originating from the same particle are imaged onto a single point, which results in particle image blur.

Light rays within a cone (at increments of 0.5º in azimuth direction and $4{\cdot}10^{-3}$ degrees in radial direction), representing the light captured by the imaging optics, are traced from the particle to the imaging optics for a range of particle positions relative to the shock. The maximum angle with respect to the cone axis α_{max} depends on the selected objective *f*/# and is given by:

$$\tan \alpha_{\max} = \frac{1}{2 f_{\#} \left(\frac{M+1}{M} \right)} \tag{1}$$

where M = 0.27 is the optical magnification, which is constant in the present study. The focal length f = 60 mm. From the ray-tracing data the geometrical shape or light intensity distribution $I(x)$ of the particle image is determined from the local light ray density and after convolution with the diffraction spot the final particle image is obtained (Figure 3). The diffraction spot diameter d_{diff} in POF coordinates (the location of the first dark band) is given by:

$$d_{diff} = 2.44 f_{\#} \left(\frac{M+1}{M} \right) \lambda \tag{2}$$

where λ = 532 nm is the wavelength of the scattered light. Simulations are carried out for θ ranging from –2 to 2 degrees and *f*/# from 8 to 22 and the distance between the measurement plane and the tunnel window is 140 mm (the dimensions of the transonic-supersonic wind tunnel (TST-27) of the Aerodynamics laboratories at Delft University of Technology). The density before the shock is 0.6 kg/m^3 and increases by 0.3 kg/m^3 over the shock.

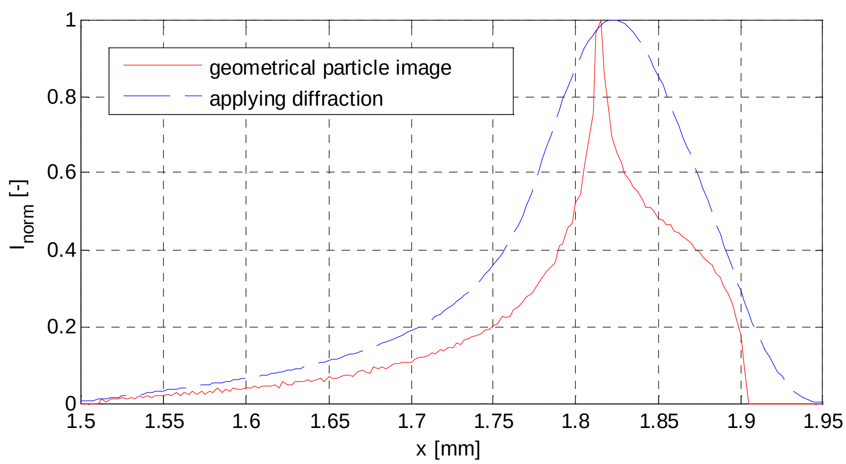

Figure 3: Blurred particle image light distribution simulation. The particle image intensity profile according to geometrical optics (solid red line) and including light diffraction due to the imaging through a finite aperture (dashed blue line).

The simulation results show that the particle images can be divided into four types (Figure 4). The first type is the undistorted particle image, which is formed when the particle is at a large distance from the shock such that none of the light rays intersect the shock. The second type, opposed to the previous one, results when all rays cross the shock. The distorted particle image is characterized by an asymmetrical stretching in the direction normal to the shock (skewed directional blurring).

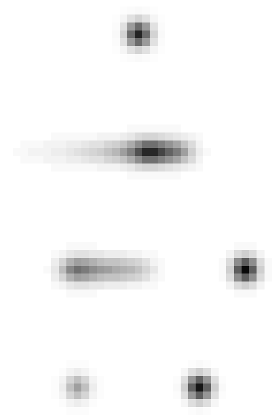

Figure 4: Four types of particle images near shock waves. The shock is oriented vertically, high density side on the right.

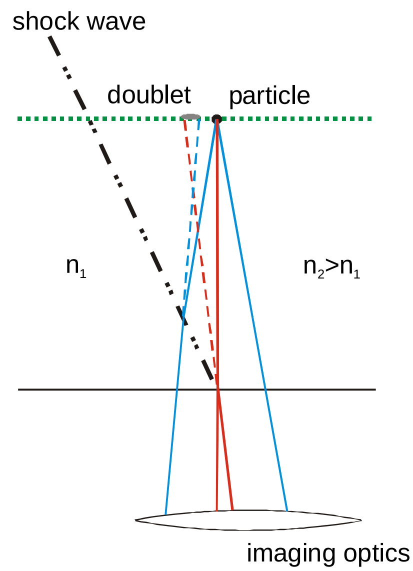

Figure 5: Schematic of particle doublet formation (refraction type).

Type three and four are particle doublets, which are formed when part of the rays intersect the shock and are in that respect end-effects (Figure 5). The particle on the high-density side (the right particle image in Figure 4) is the sharply imaged undistorted component and the low-density side particle image (the doublet) is the results of either refraction or reflection forming type three or four respectively. For type three the doublet itself is skewed and directionally blurred as type two. Figure 5 shows an example where the left half of the light cone is deflected by the shock forming the doublet (identical to the situation in figure 2), while the right half is unaffected. For type four the particle is on the high-density side and the rays intersect at a small angle, below the limit angle for total internal reflection (0.7 degrees for the present density level). The shock acts as a mirror and the doublet is also sharply imaged. Because doublets are local (end-) effects, the skewed and direction blurring of particle images generally dominate in PIV.

3. EXPERIMENTAL VALIDATION

To validate the particle images shapes as predicted by the simulation a PIV experiments was performed in the TST-27 supersonic wind tunnel. A planar bow-shock wave from the 2D wedge-plate model (Scarano and Van Oudheusden 2003) was measured using an experimental configuration corresponding to that of the numerical simulation (Figure 2). The Mach 1.96 free stream flow expanded from 1.94 bars stagnation pressure at ambient temperature yields a free-stream velocity of 500 m/s and density of 0.56 kg/m^3. The model spans the width of the test section (280 mm) and consists of a wedge with sharp leading edge imposing a flow deflection of 11.3 degrees. The resulting oblique shock wave has an angle of 41 degrees with respect to the free stream. The flow velocity is decreased to 440 m/s and the density increases to 0.86 kg/m^3. The wedge is followed by a plate 50 mm long and 20 mm thick truncated with a sharp base. The flow is seeded with 50 nm TiO_2 particles, which are illuminated by a double pulse Nd:YAG laser (400 mJ per pulse) in a 1 mm thick light sheet. The pulse duration and separation are 6 ns and 0.6 μs respectively. A 12-bit CCD camera equipped with a Nikon 60 mm objective is used to record the images at 1376×432 pixels resolution corresponding to a field of view of 35x11 mm^2. The camera can be translated and rotated in the horizontal plane to control the viewing direction. So instead of changing the flow, i.e. the orientation of the shock, as done in the numerical simulation, the imaging optics are moved, which is equivalent for small viewing angles. The viewing angle with respect to the shock is obtained from the goniometric relation $\sin\theta = \sin\sigma \sin\theta_x$, in which $\sigma = 41°$ is the shock angle with the horizontal direction and θ_x is the angel of rotation of the camera.

Figure 6 shows for $\theta = -1.3°$ and *f*/16 that the particle image is blurred in the direction normal to the shock. As expected the particle image is directionally blurred and skewed near the shock resembling the shape of the blurred particle image found in the numerical simulation (Figure 4, see also section 4).

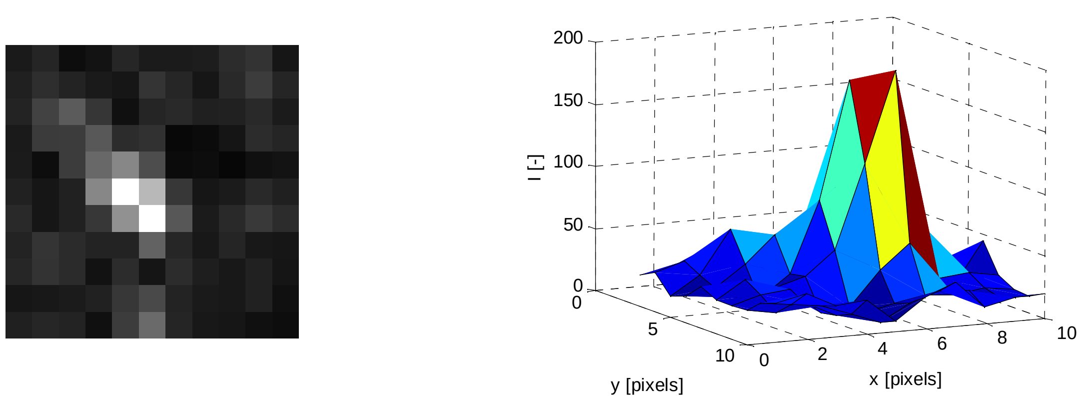

Figure 6: Skewed directional blur observed in a real PIV recording (left) and corresponding intensity map (right).

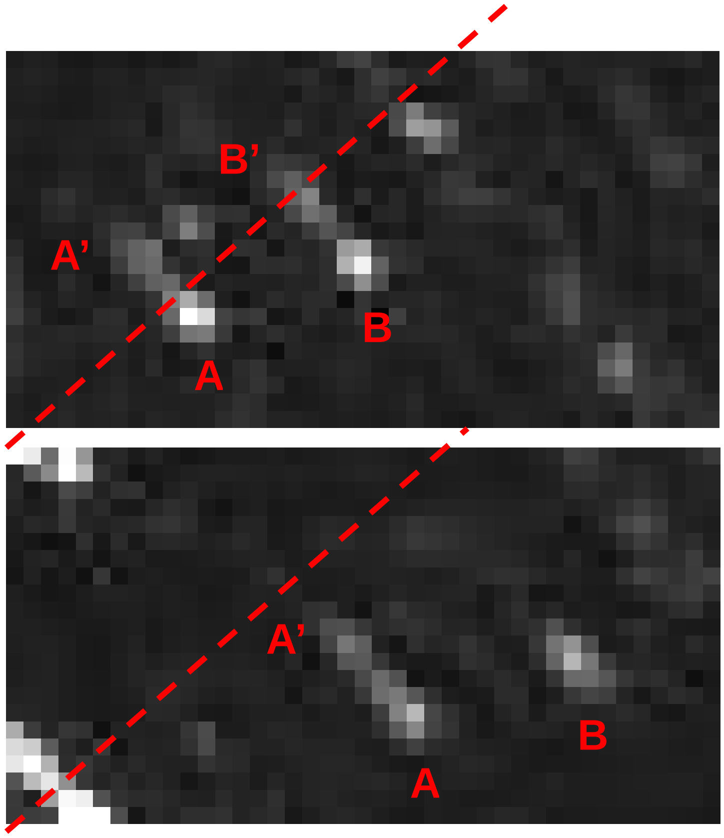

Figure 7: Two particle image doublets (A' and B') observed in a PIV recording (upper: first exposure, lower: second exposure separated in time by 0.6 µs). The dashed line indicates the shock orientation.

Figure 7-upper shows for θ = -0.65º and *f*/16 two refraction type doublets A' and B' corresponding to particles A and B. That these are doublets and not just two individual particles can be concluded observing the second exposure (lower image in Figure 7) recorded 0.6 µs after the first. Due to the flow velocity the particles have been displaced by approximately 0.30 mm (12 pixels). As mentioned above the phenomenon of doublet particle images occurs only locally under specific circumstances. After displacement, particle B has moved out of this region and therefore its doublet B' is no longer seen and image B is of the skewed directional blur type (similar to Figure 6). Conversely, particle A is still imaged as a doublet although the ratio of the two peak intensities and their relative location have changed. Note also that a new doublet appears in the lower left corner near the dashed line due to the appearance of another particle tracer.

The skewed directional blur and the refraction type doublets have been found to exist in actual PIV recordings validating the modeling of particle imaging across shocks. The existence of reflection type doublets, however, has not yet been confirmed by experimental evidence.

4. RESULTS

In the analysis of the simulation results the focus is on the case where all light rays intersect with the shock resulting in skewed directional blurring of the particle. In section 4.3 will be shown that the refraction type particle doublet can be seen as a special case of the former type of particle image blur. The shape and size of particle image will be discussed in relation to the two basic angles involved: the viewing direction with respect to the shock θ and the half angle α_{max} of the light cone considered (Eq. 1), which is represented by $f_{\#}\left(\frac{M+1}{M}\right)$ or *f/#*, since *M* is constant in the present study. Furthermore from Figure 2 it is seen that the incidence angles of all light rays with the shock and consequently the deflection angles do not change with the position of the particle (for given θ and *f/#*), so that the geometrical blur length scales linear with the distance between the particle and the shock in viewing direction Z_D and its shape (intensity distribution) is independent of Z_D. Therefore the direction normal to the shock x is normalized as $x_{norm} = \frac{x - x_p}{Z_D}$, where x_p is the actual particle position. X_{norm} represents (but is not fully identical to) the light ray deflection angle. The simulation results show that the normalized standard deviation σ/Z_D and the skewness of the geometrical intensity distribution are indeed constant, which verifies that the geometrical blur shape is independent of Z_D. The skewness is the normalized third moment of the intensity distribution (seen as the probability density function) in x and is defined as:

$$skewness = \frac{E(x-\mu)^3}{\sigma^3} \tag{3}$$

where μ is the mean and σ is the standard deviation. Values for σ/Z_D and the skewness are presented in tables 1 and 2. For θ = 0, 0.5, 1 and part of –0.5 degrees no region exist where all light rays are deflected by the shock, hence no data is available for those angles. After applying diffraction the particle image shape does become dependant on the particle location.

Table 1: Normalized standard deviation σ/Z_D of the geometrical particle shape ($\cdot 10^{-3}$)

θ (deg)	**f/8**	**f/11**	**f/16**	**f/22**
-2	0.86	0.57	0.37	0.27
-1	5.53	2.57	1.44	0.98
-0.5	x	x	6.60	3.33
2	1.04	0.67	0.43	0.31

Table 2: Skewness of the geometrical particle shape

θ (deg)	**f/8**	**f/11**	**f/16**	**f/22**
-2	-1.28	-0.90	-0.61	-0.44
-1	-3.18	-1.84	-1.17	-0.82
-0.5	x	x	-2.79	-1.61
2	-1.46	-1.00	-0.67	-0.48

4.1. Effect of the *f*/#

Figure 8 presents the geometrical and diffracted particle images returned for θ = -2° and varying *f/#*. As expected the geometrical blur length increases with decreasing *f/#* (larger range of intersection angles with the shock, Eq. 1) resulting in a distinct tail in the geometrical profile in the direction of lower density (left side) for *f*/8. However the diffraction spot (Eq. 3) increases in size with *f/#* and therefore little difference is observed when the diffractive effect is included (Figure 8-right). Only the tail for *f*/8, and to a lesser extent for *f*/11, is still visible. Note however that in the *y*-direction (parallel to the shock and normal to *x*) the width of the particle is still determined by the diffraction spot, so that the amount of blur perceived is different: for decreasing *f/#* the particle image appears to be more stretched even though in the *x*-direction the particle shapes are similar.

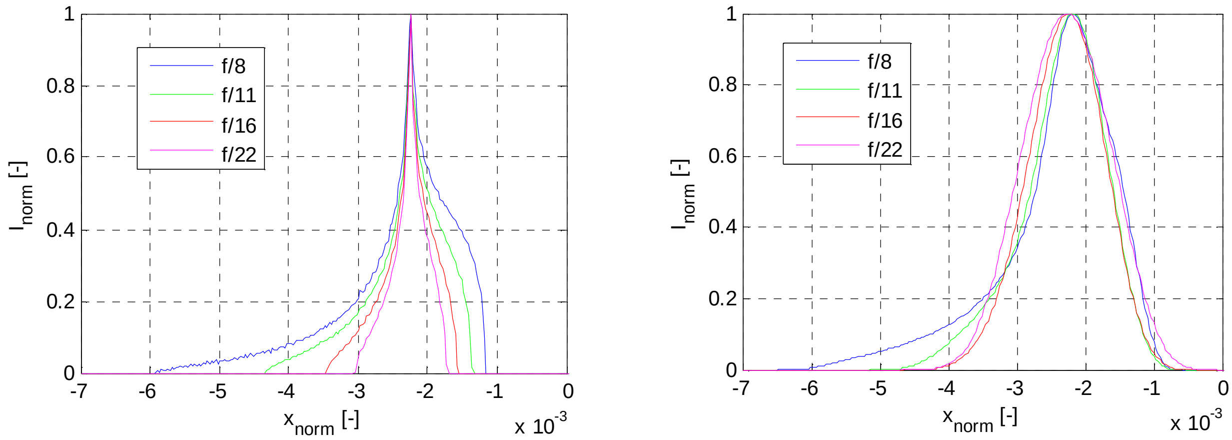

Figure 8: The effect of *f/#* on the skewed directional image blur for θ = -2° and particle located at Z_D = 83 mm (Left: geometrical particle image, Right: including diffraction effects).

To determine the particle image blur length from actual PIV recordings, the particle image recordings auto-correlation peak width is evaluated. In this case the peak intensity R is assumed to be of elliptical Gaussian shape expressed by

$$R(r,s) = e^{\frac{1}{2}\left(\left(\frac{r}{\sigma_r}\right)^2 + \left(\frac{s}{\sigma_s}\right)^2\right)} \tag{4}$$

A 3×3 kernel around the auto-correlation maximum is used to fit the expression, where the coordinates r and s are taken along the principal axes of the ellipse with s in the direction normal to the shock. The standard deviation σ_s is the measure for the peak width/stretching and the particle image blur length. An auto-correlation window size of 31×31 pixels with 50% overlap is used. The correlation maps are averaged over 300 realizations. Figure 9 shows σ_s for θ = -1.3 deg. Particle image blur is observed between s = -3.5 and –1 mm. As predicted by the simulation, the correlation peak width, hence blur length, at these conditions is independent of *f/#* (except for *f/*8), which again validates the modeling of the particle imaging.

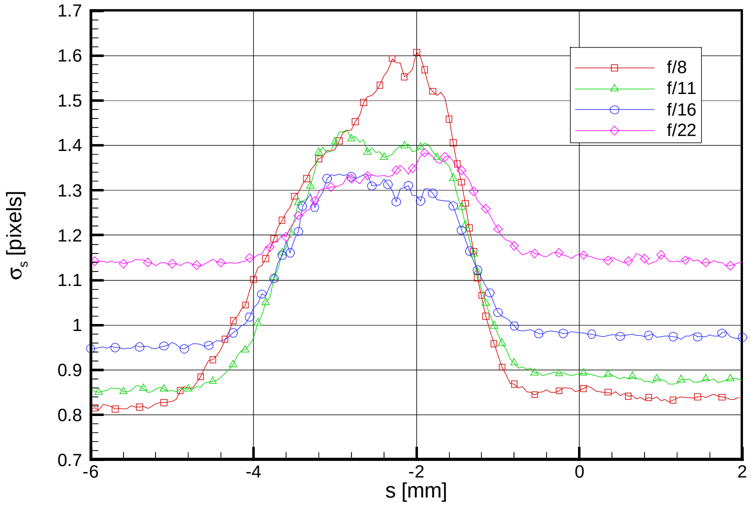

Figure 9: The effect of *f/#* on the auto-correlation peak width.

4.2. Effect of the viewing angle

Figures 10 and 11 show the blurred particle images for θ = -1 and +2 degrees respectively. Compared to θ = -2° the geometrical blur length has grown considerably for θ = -1°, due to an increase in the deflection angle for smaller incidence angles with respect to the shock. The left side of the profile has expanded even more than the side right from the peak. The increase of the geometrical blur length and skewness with decreasing viewing angle is further illustrated in Tables 1 and 2. The diffraction profiles however show again great similarity near the peak intensity, because the skewed direction blurring occurs only at small Z_D for the present geometry (Figure 2) resulting in small geometrical blur compared to the diffraction spot. Comparing Figure 8 and Figure 11 (θ = -2° and +2° respectively) the intensity profile is almost identical, although the blur length is slightly larger for positive viewing angles, which is also seen from table 1.

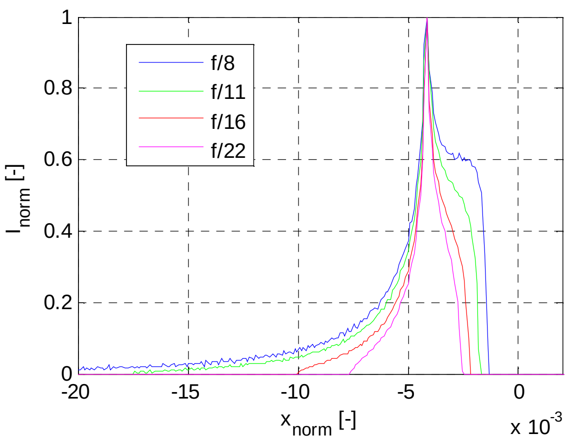

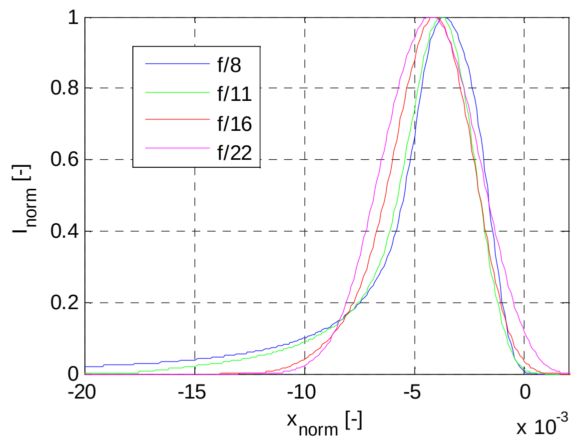

Figure 10: Skewed directional image blur for θ = -1° and particle located at Z_D = 25 mm (Left: geometrical particle image, Right: including diffraction effects).

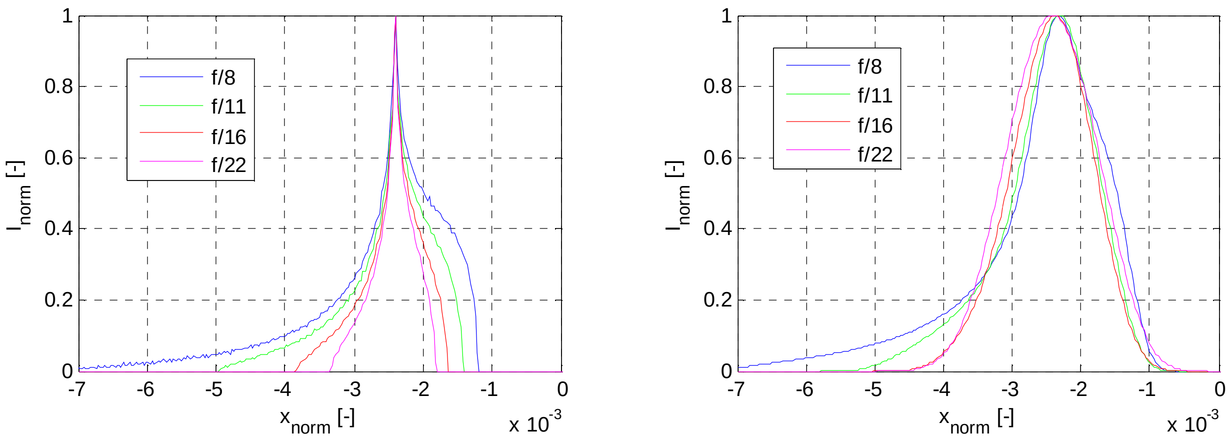

Figure 11: Skewed directional image blur for θ = +2° and particle located at Z_D = 83 mm (Left: geometrical particle image, Right: including diffraction effects).

4.3. Particle doublets

An example of a particle doublet obtained from the simulation is presented in Figure 12 (θ = -2°). Compared to the skewed directional blurring (Figure 8) the geometrical profile is cut off on the left side, while the remaining part of the profile is left unchanged. The light rays that are expected in the left tail are not intersecting the shock and appear at the actual particle location in the image (x_{norm} = 0). This demonstrates that the geometrical particle profiles obtained for skewed directionally blurred image particles described above are also useful to describe doublets.

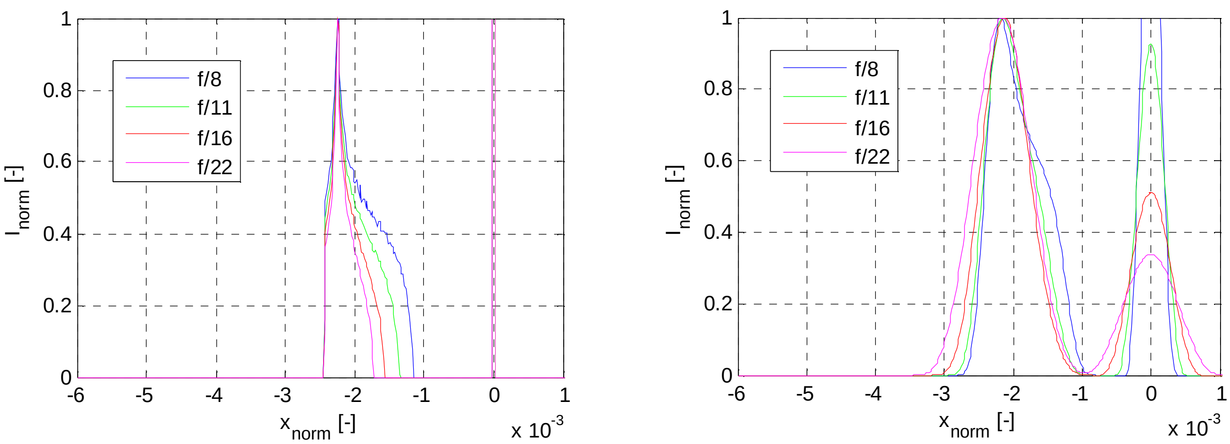

Figure 12: Particle doublets for varying *f/#* and θ = -2° and Z_D = 134 mm (Left: geometrical particle image, Right: including diffraction effects).

5. CONCLUSIONS

A model has been introduced that describes particle imaging through a shock wave. The geometrical image is constructed first based on light ray tracing within a finite light cone. After a convolution of the geometrical particle image with the diffraction spot of the imaging system the particle image is obtained as it is actually recorded. The returned blurred particle images could be divided into 3 characteristic shapes: skewed directional blur, particle doublet due to refraction and particle doublet due to total internal reflection. The existence of the first two types was confirmed by experiments. The shape of skewed direction blurred images was presented for varying viewing directions and numerical apertures. And furthermore it was shown that the particle doublet shape could be inferred from the basic shape of the skewed direction blurred image.

Knowing the characteristic shape for a blurred particle near a shock the effect of particle blur on PIV measurements can be investigated. Moreover particle images needed for stronger and possibly curved shock waves and for a larger range of viewing angles.

ACKNOWLEDGEMENTS

This work is supported by the Dutch Technology Foundation STW under the ‘VIDI Vernieuwingsimpuls’ program grant DLR.6198.

REFERENCES

Abart JC, Molton P, Maury B, Jacquin L (2004) Implantation de la PIV dans la soufflerie transsonique S3Ch. *9e congrès francophone de vélocimétrie laser*, Brussels, Belgium, paper K.2

Elsinga GE, van Oudheusden BW, Scarano F (2005) Evaluation of aero-optical distortion effects in PIV. *Accepted for Exp Fluids*, DOI: 10.1007/s00348-005-1002-8

Raffel M, Kost F (1998) Investigation of aerodynamic effects of coolant ejection at the trailing edge of a turbine blade model by PIV and pressure measurements. *Exp Fluids* 24: 447-461

Raffel M, Willert CE, Kompenhans J (1998) *Particle Image Velocimetry: A practical guide*. Springer, Berlin Heidelberg New York

Scarano F, Van Oudheusden BW (2003) Planar velocity measurements of a two-dimensional compressible wake. *Exp Fluids* 34: 430-441

Sutton GW (1985) Aero-optical foundations and applications. *AIAA J* 23 10